

# Coupled patterns of spatiotemporal variability in Northern Hemisphere sea level pressure and conterminous U.S. drought

Zhijia Zhang and Michael E. Mann

Department of Environmental Sciences, University of Virginia, Charlottesville, Virginia, USA

Received 12 April 2004; revised 8 July 2004; accepted 20 September 2004; published 4 February 2005.

[1] We apply the multitaper frequency domain–singular value decomposition signal detection method to the investigation of coherent patterns of variation in seasonal Northern Hemisphere sea level pressure and conterminous U.S. summer drought during the period 1895–1995. The analysis identifies statistically significant patterns of spatiotemporal variability on interannual and bidecadal timescales indicative of both cold-season and warm-season atmospheric influences on North American drought patterns. The most robust signal found appears to be associated with the influences of the El Niño–Southern Oscillation (ENSO) on North American summer drought. Evidence is also found to support the existence of a roughly bidecadal drought signal tied to warm-season atmospheric circulation changes. The “Dust Bowl” conditions of the 1930s appear to result from a combination of these bidecadal influences on drought conditions that coincide with a decrease in the amplitude of interannual ENSO-related variability during the 1930s.

**Citation:** Zhang, Z., and M. E. Mann (2005), Coupled patterns of spatiotemporal variability in Northern Hemisphere sea level pressure and conterminous U.S. drought, *J. Geophys. Res.*, *110*, D03108, doi:10.1029/2004JD004896.

## 1. Introduction

[2] A sizable body of research over the past 2 decades has involved the analysis of atmospheric, oceanic, and hydroclimatic data using frequency domain signal detection methods to isolate oscillatory signals in the climate system on interannual and decadal timescales [e.g., Barnett, 1991; Ghil and Vautard, 1991; Mann and Park, 1993, 1994, 1996, 1999; Allen and Smith, 1994; Dettinger et al., 1995; Mann et al., 1995a, 1995b; Lall and Mann, 1995; Jiang et al., 1995; Rajagopalan et al., 1998a; Moron et al., 1998; White and Cayan, 1998; Minobe, 2000; Park and Mann, 2000; Turre et al., 2001; Venegas et al., 2001; Ribera and Mann, 2002, 2003]. Such signals offer potential prospects for skillful long-term predictability [Keppenne and Ghil, 1992; Rajagopalan et al., 1998b].

[3] Many of these frequency domain analyses [e.g., Barnett, 1991; Keppenne and Ghil, 1992; Jiang et al., 1995; Dettinger et al., 1995; Park and Mann, 2000; Turre et al., 2001; Ribera and Mann, 2002, 2003] have focused on interannual signals associated with the El Niño–Southern Oscillation (ENSO). Other time-domain- or correlation-based statistical analyses have identified relationships between atmospheric circulation changes associated with ENSO and U.S. summer drought [Rajagopalan et al., 2000; Gershunov and Barnett, 1998; Cole and Cook, 1998; Dai and Trenberth, 1998; Barlow et al., 2001]. To our knowledge, however, no previous analyses have examined the

frequency domain structure and evolving patterns of covariability between the large-scale atmospheric circulation and continental drought.

[4] Such is the purpose of this study. We investigate patterns of covariability between conterminous U.S. drought and Northern Hemisphere atmospheric circulation patterns through application of the multitaper frequency domain–singular value decomposition (MTM-SVD) approach of Mann and Park [1996, 1999]. The MTM-SVD methodology has been successfully applied to the investigation of spatiotemporal oscillatory signals in instrumental, proxy, and climate model data sets (see the review by Mann and Park [1999]), including, as here, applications to coupled patterns of evolution in two or more climate fields [Mann and Park, 1996; Delworth and Mann, 2000; Minobe, 2000; Venegas et al., 2001; Turre et al., 2001; Ribera and Mann, 2002, 2003; Turre and White, 2003]. The MTM-SVD analysis is applied to seasonal sea level pressure data over the Northern Hemisphere and the Palmer Drought Severity Index (PDSI) over the conterminous United States over the interval 1895–1995. Our analysis reveals signals on interannual and bidecadal timescales. We focus on the most robust of these signals, which appears to be associated with the influence of interannual ENSO variability.

## 2. Data

### 2.1. PDSI Data

[5] We make use of summer (June–August) PDSI estimates available from 1895 to 1995 over the conterminous United States [Cook et al., 1999]. The gridded estimates are

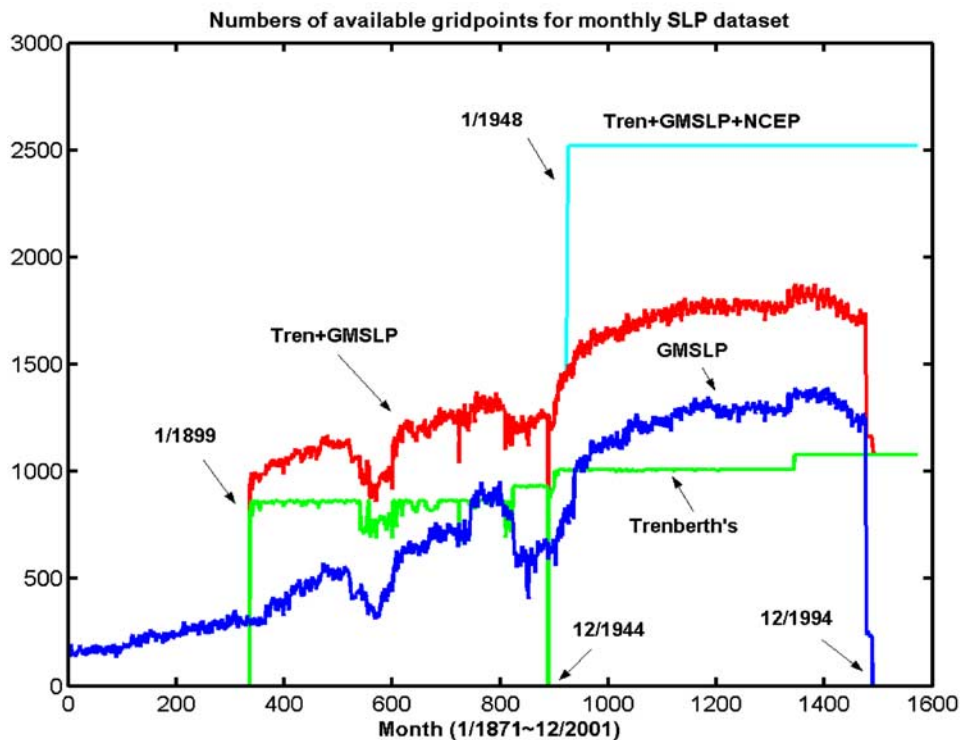


**Figure 1.** Temporal structure of available monthly sea level pressure (SLP) data based on combination of available data sets: TrenSLP (green), GMSLP (dark blue), and TrenSLP plus GMSLP (red). All spatial gaps evident during January 1948 through December 2000 are filled with National Centers for Environmental Prediction (NCEP) data as described in text.

based on a nearest-neighbor gridding scheme applied to a  $2^\circ$  latitude by  $3^\circ$  longitude grid. While other drought metrics are available, the PDSI provides a useful assessment of dry or wet spells of weather through the incorporation of a statistical hydrological balance model that incorporates temperature and precipitation information and serial persistence in its definition [Palmer, 1965]. The PDSI is standardized to provide a similar relative measure of drought across hydroclimatically distinct regions, with negative (positive) values indicative of dry (wet) conditions and with values generally falling between  $-6$  and  $+6$ . Extensions of summer PDSI estimates over the conterminous United States are available in data back to 1700 based on drought-sensitive tree ring data [Cook *et al.*, 1997, 1999; Zhang *et al.*, 2004].

## 2.2. Global Sea Level Pressure Data

[6] We also make use of sea level pressure (SLP) data over the Northern Hemisphere region spanned by the Pacific, North America, and the Atlantic ( $0^\circ\sim 85^\circ\text{N}$ ,  $180^\circ\sim 5^\circ\text{W}$ ). This subregion of the Northern Hemisphere is chosen for its relevance to atmospheric circulation regimes influencing North America and the conterminous United States. We employ boreal warm half-year (May–October) and cold half-year (November–April) seasonal averaging windows. The use of 6 month seasonal averaging windows in this study is motivated by two considerations. Such half-year seasonal means appear to represent an optimal compromise [see Trenberth and Hurrell, 1994] between the nonstationarity of the seasonal cycle (favoring

shorter seasonal averaging intervals) and the requisite statistical constraint in evaluating a seasonal mean (favoring longer seasonal averaging intervals). Moreover, since networks of proxy data available in past centuries, prior to the instrumental record, typically only provide adequate resolution of broadly defined seasonally integrated climate changes, such a resolution into half-year seasons establishes a baseline that should be useful for similar, subsequent studies employing proxy-based reconstructions of past atmospheric circulation and continental drought variability. Use of shorter (3 month) winter (December–January–February) and summer (June–July–August) seasons leads to no significant differences in our conclusions. For example, the estimated composite patterns for ENSO warm events (as discussed in section 4) are spatially correlated at  $r = 0.99$  for cold season/winter and  $r = 0.95$  for warm season/summer.

[7] The SLP estimates used in this study are derived through a combination of several distinct data sources providing complementary spatial and temporal sampling (see Figure 1). These data sources include (1) Northern Hemisphere  $5^\circ \times 5^\circ$  gridded ( $15^\circ\sim 85^\circ\text{N}$ ,  $0^\circ\sim 335^\circ\text{E}$ ) monthly SLP estimates available back to 1899 based on a combination of daily instrumental measurements and digitized hand-drawn analyses [Trenberth and Paolino, 1980] (hereinafter “TrenSLP”), (2) global  $5^\circ \times 5^\circ$  gridded historical monthly SLP estimates covering the period 1871–1994 based on in situ marine and land station SLP observations, blended with gridded analyses [Basnett and Parker, 1997] (hereinafter “GMSLP”), and (3) global  $5^\circ \times 5^\circ$

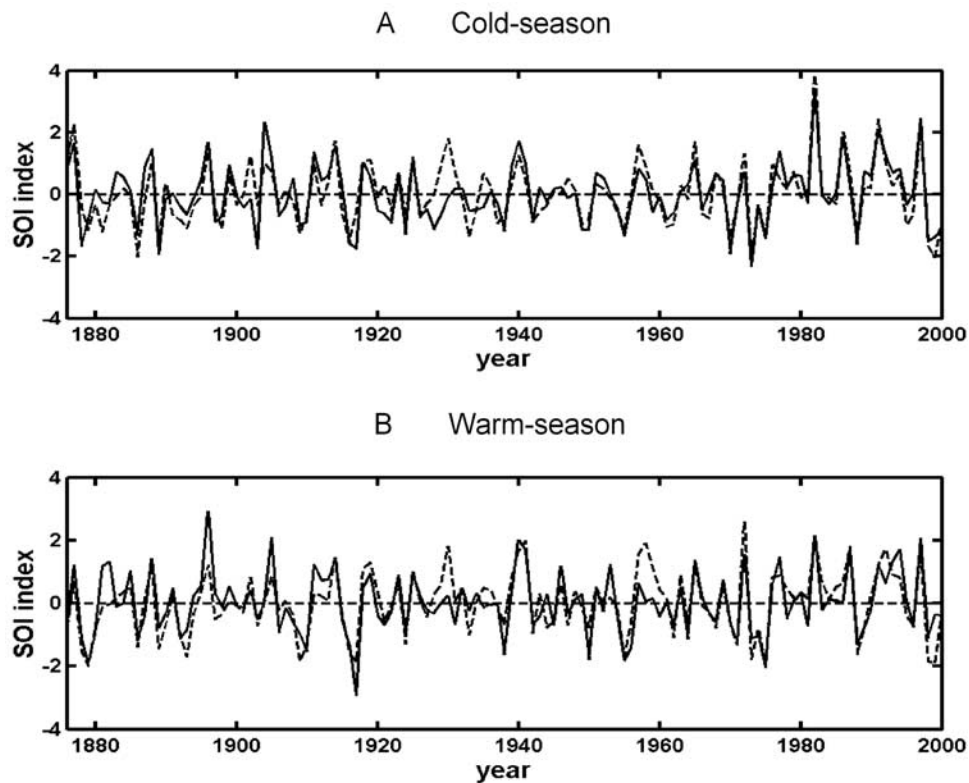


**Figure 2.** Station-based seasonal Southern Oscillation Index (SOI) (solid line) and seasonal SOI (dashed line) based on regularized expectation maximization method infilled global SLP network over tropical Pacific region for both (a) cold season and (b) warm season. Indices are normalized on the basis of standardized deviation over 1876–2000 with a reversed value shown.

gridded monthly SLP developed under the National Centers for Environmental Prediction (NCEP)/National Center for Atmospheric Research Reanalysis Project, which employs a state-of-the-art analysis/forecast system to assimilate and spatially infill meteorological observations back to 1948 [Kalnay *et al.*, 1996] (hereinafter “NCEP SLP”). The three data sets were merged into a global  $5^\circ \times 5^\circ$  data set for the boreal cold-season and warm-season half-year means. The procedure involved merging the TrenSLP and GMSLP data sets (which are on a commensurate global  $5^\circ$  latitude by  $5^\circ$  longitude grid) into a single composite global SLP data set back to 1871, albeit one with substantial spatial and temporal gaps. This incomplete data set was then calibrated against the globally complete NCEP SLP data set over the more recent interval 1948–1994 to produce a globally infilled SLP data set back to 1871. In this step the NCEP data are used effectively to spatially interpolate the information in the merged TrenSLP/GMSLP data set, with the fidelity of any long-term variability and trends contained in the original data sets implicitly retained. The possibility of spurious trends in the shorter NCEP data set is thus unlikely to impose any bias on the resulting spatial infilling. The infilling process does assume that the patterns of spatial covariance between the NCEP and merged TrenSLP/GMSLP data during the data-sparse intervals are similar to those captured within the modern (1948–1994) calibration period. Such assumptions appear to be generally valid on the basis of analogous spatial

infilling experiments using data fields from control and forced climate model simulations [Rutherford *et al.*, 2003; Zorita *et al.*, 2003].

[8] The infilling with NCEP data was performed using the regularized expectation maximization method (“RegEM” [Schneider, 2001; Mann and Rutherford, 2002; Rutherford *et al.*, 2003; Zhang *et al.*, 2004]), which is an iterative method for estimating missing data through the estimation of means and covariances from an incomplete data field. The RegEM method is analogous to other methods [e.g., Smith *et al.*, 1996; Kaplan *et al.*, 1997, 1998, 2000] of climate field reconstruction (CFR), in which missing spatial data are estimated from sparse early data through relating the patterns evident in the sparse, longer data interval to the patterns defined by the empirical eigenvectors estimated from a shorter, data-rich interval during which complete or nearly complete spatial information is available. Kaplan *et al.* [2000] used the latter such method to similarly reconstruct patterns of historical SLP back through the late nineteenth century. As RegEM makes more complete use of the available spatiotemporal information in the reconstruction process [see Schneider, 2001] and performs well even in the presence of nonstationary behavior [Rutherford *et al.*, 2003], we, however, favor the use of this particular variant of CFR for the infilling of historical SLP patterns from the available instrumental data. In contrast to Kaplan *et al.* [2000], who make use purely of historical SLP observations in the infilling process, we

make use of the NCEP SLP estimates for a more spatially complete representation of the modern observations. One additional caveat in the interpretation of the resulting spatially complete data set is that certain regions are infilled on the basis of model physics rather than actual observations. Nonetheless, previous analyses of the NCEP data [Ribera and Mann, 2002, 2003] yield conclusions regarding the patterns of interannual variability over the past half century (and changes therein) that are consistent with the conclusions of independent studies making use of in situ observations.

[9] In this study, we only make use of the SLP data back to 1895. The skill of this statistical infilling was established through statistical cross-validation tests. These tests indicate broadly skillful reconstructions of SLP over the regions considered in this study (Northern Hemisphere and tropics) and more questionably skillful reconstructions over the Southern Ocean and high latitudes of the Southern Hemisphere, regions which are not considered in this study. As an example test of the fidelity of the statistical infilling procedure, we consider the tropical Pacific region, for which the data are fairly sparse prior to 1948. Similar to Newman *et al.* [2004], who generate an ENSO as the leading empirical orthogonal function (EOF) of monthly sea surface temperature (SST) in the region 20°N to 20°S, 120°E to 60°W, we generate a Southern Oscillation Index (SOI) as the leading EOF of our infilled SLP over the same region. We compared the resulting index to a station-based SOI [Nicholls, 1988] over both the boreal cold and warm half years. In developing the EOF-based SOI we removed the four grid points surrounding Darwin (131°E, 12°S) and the four grid points surrounding Tahiti (149°W, 17°S) to insure that the resulting index was statistically independent of the information that contributed to the station-based index. The resulting reconstruction indicates quite skillful reconstruction of the station-based SOI from the EOF-based index ( $r = 0.72$  and  $r = 0.80$  for cold and warm seasons, respectively) during the data-sparse interval 1876–1948 (see Figure 2).

### 3. Methods

[10] The MTM-SVD method [Mann and Park, 1994] (see the review by Mann and Park [1999]) is used in the detection of spatiotemporal oscillatory signals in one or several simultaneous climate data fields. Previous applications of the method include analyses of instrumental climate fields [Mann and Park, 1994, 1996; Mann *et al.*, 1995a; Minobe, 2000; Venegas *et al.*, 2001; Tourre *et al.*, 2001; Tourre and White, 2003], proxy climate data and proxy-based climate reconstructions [Mann *et al.*, 1995b; Delworth and Mann, 2000; Mann *et al.*, 2000], model reanalysis data [Ribera and Mann, 2002, 2003], coupled model integrations [Delworth and Mann, 2000], and synthetic forecasting experiments [Rajagopalan *et al.*, 1998b].

[11] The MTM-SVD method identifies distinct frequency bands within which there is a pattern of spatially coherent variance in the data that is greater in amplitude than would be expected under the null hypothesis of spatiotemporal colored noise (see, e.g., Mann and Park [1999] for a

thorough review). The method differs from conventional EOF-based approaches [e.g., Wallace and Gutzler, 1981; Horel, 1981] in that both phase information and amplitude information are retained in the data decomposition, and the method differs from complex EOF approaches in that any patterns isolated are intrinsically band limited [see Mann and Park, 1999]. The MTM-SVD method provides a natural description of a narrowband, but not necessarily strictly periodic, spatiotemporal signal in a multivariate data set. In MTM-SVD the underlying time series model allows for phase and amplitude modulation, providing a natural description of climate signals that may not be periodic but instead exhibit the irregular oscillatory behavior expected in association with internal modes of variability that have preferred intrinsic timescales but that are perhaps only intermittently excited through stochastic or external forcing [see Mann and Park, 1999].

[12] Once a signal is detected with the method (through examination of the “local fractional variance” spectrum or “LFV” spectrum [see Mann and Park, 1999]), both its temporal history and characteristic evolving spatial pattern can readily be reconstructed. Consistent with previous applications of MTM-SVD [see Mann and Park, 1999] we used a bandwidth parameter  $NW = 2$  and  $K = 3$  tapers. For 101 years of data as used in this study this admits a nominal bandwidth of  $\pm 0.02$  cycles/yr, though peaks can potentially be distinguished at the finer resolution of the Rayleigh frequency of  $\pm 0.01$  cycles/yr (see discussion by Mann and Park [1999]). A maximum resolvable periodicity of 50 year timescale can be resolved from secular trends in the data. Confidence levels were estimated by the bootstrap procedure described by Mann and Park [1999], invoking the null hypothesis of a smoothly varying colored noise background.

[13] The MTM-SVD analysis was applied to the joint SLP/PDSI data set over the common interval 1895–1995 separately using both warm-season and cold-season SLP. Employing these paired analyses allowed for separate investigation of potentially distinct antecedent cold-season and coincident warm-season atmospheric influences on summer drought. The LFV spectra were analyzed both for the full (101 year) joint data set and in an “evolutionary” fashion employing a 40 year moving window [see Mann and Park, 1996; Ribera and Mann, 2002, 2003] to detect potential time dependence in the amplitude and frequency characteristics of interannual signals in the data. Additional MTM-SVD analyses were performed separately on the summer PDSI and seasonal SLP fields, to investigate the robustness of detected signals with respect to the particular field analyzed. In each of these analyses, grid point series were first standardized by removal of the long-term mean and normalization by the long-term standard deviation. As in previous MTM-SVD analyses of coupled fields [e.g., Mann and Park, 1996; Delworth and Mann, 2000; Ribera and Mann, 2002, 2003], the standardized grid point data (648 SLP grid points and 155 PDSI grid points) were then weighted so that the two fields contribute equal overall variance in the analysis. SLP data were then areally weighted to account for the large variation in areal representativeness of the grid point data as a function of latitude. The additional single time series of the boreal cold-season SOI [Nicholls, 1988] was added to the

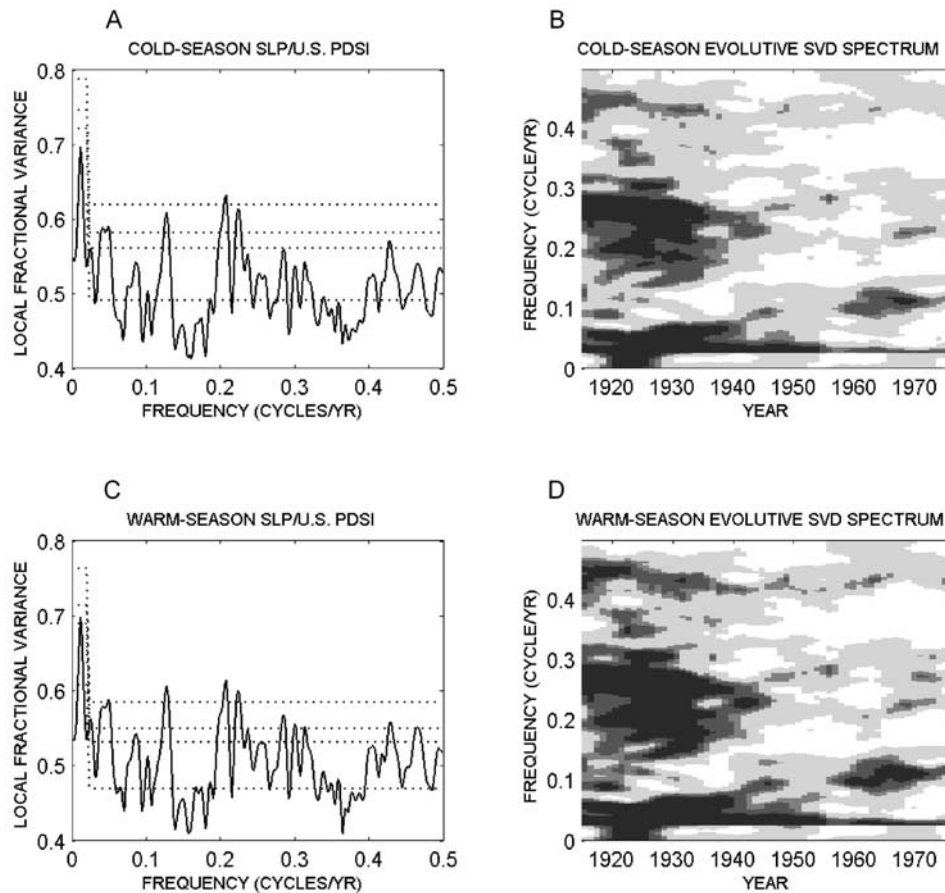


**Figure 3.** (a) Local fractional variance spectrum (1895–1995) for the joint field of cold-season sea level pressure ( $0^{\circ}\sim 85^{\circ}\text{N}$ ,  $180^{\circ}\sim 5^{\circ}\text{W}$ ) and U.S. summer Palmer Drought Severity Index (PDSI). The confidence levels (50%, 90%, 95%, and 99%) are denoted by dashed lines. (b) Evulsive singular value decomposition spectrum with a moving 40 year window for the joint field. Significance is indicated by gray scale with light to dark gray representing 50%, 90%, 95%, and 99% confidence. (c and d) As in Figures 3a and 3b but with joint climate field comprising warm-season SLP and U.S. summer PDSI.

multivariate data set to allow the phase of any signal identified to be defined relative to a conventional indicator of ENSO conditions.

#### 4. Results

[14] The LFV spectra for the joint PDSI/SLP MTM-SVD analyses employing both cold-season and warm-season SLP (Figure 3) indicate several highly significant spectral peaks on interannual timescales associated with both 2–3 year “high-frequency” and 4–7 year “low-frequency” bands of ENSO variability [e.g., Barnett, 1991; Mann and Park, 1994, 1996; Jiang et al., 1995; Ribera and Mann, 2002, 2003]. Similar timescale variability has also been established as being statistically significant on the basis of spectral analysis of PDSI data [Cook et al., 1997]. A bi-decadal (roughly 20–22 year timescale) signal, previously established in long-term reconstructions of continental U.S. drought in past centuries [see Cook et al., 1997], is also highly significant, detected at the 99% significance level for the joint PDSI/warm-season SLP analysis. This signal is statistically significant in separate MTM-SVD analyses of the warm-season SLP field only and the summer PDSI field

only but not for cold-season SLP alone. A roughly decadal timescale (7–8 year period) peak is statistically significant in the joint field analysis but not in analyses of either warm-season or cold-season SLP alone and is thus not discussed further. A marginally significant (90% level) secular variation (corresponding to timescales longer than 50 years) is also evident for both joint field analyses. Possible secular trends in the data are not, however, the focus of this analysis. The evulsive analysis employing a 40 year moving window indicates some frequency and amplitude modulation of the interannual variability over time. The evulsive analysis suggests a breakdown of interannual oscillatory variability in the 1930s but with a persistence of decadal variability, perhaps contributing to the sustained “Dust Bowl” drought conditions of the 1930s evident in the contemporaneous U.S. PDSI data [e.g., Cook et al., 1999]. This connection is further discussed below.

[15] We choose first to focus on the characteristics of the bi-decadal drought signal associated with the 20–22 year timescale peak in the LFV spectra. As discussed above, the signal appears to be associated with warm-season atmospheric circulations, with no corresponding signal apparent in the cold-season SLP field. It has been speculated that this

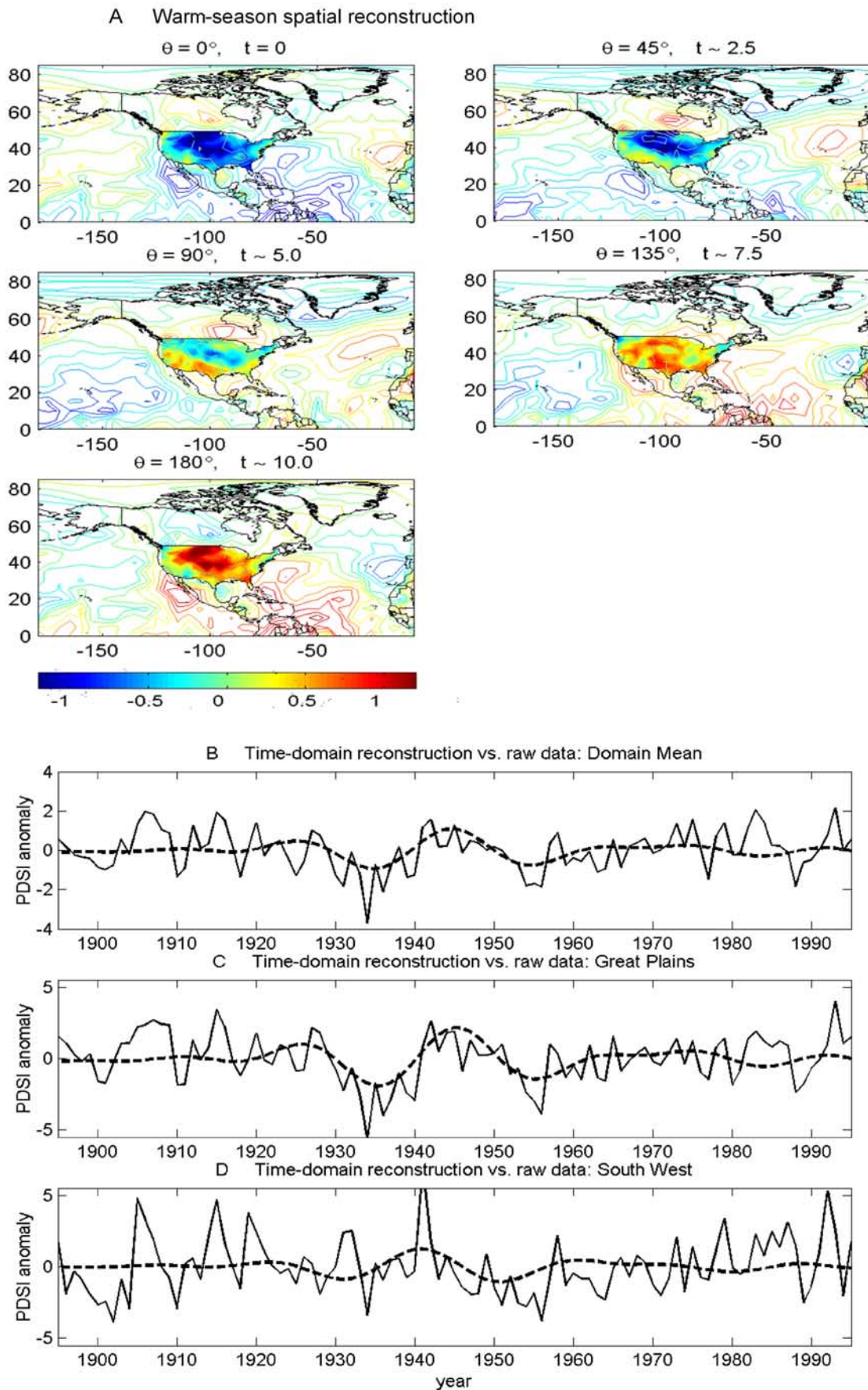


Figure 4

signal could be related to 22 year timescale solar forcing. We do not seek to test such a causal connection here, but, as *Cook et al.* [1997] did, we simply note that a statistically significant bidecadal signal does appear to be present in the data and seek to describe its temporal and spatial characteristics. Investigation of the possibility that this lower-frequency signal (or the secular variation isolated in the MTM-SVD analysis) modulates the characteristics of the higher-frequency interannual variability discussed later would be a worthy extension of the present analysis but is beyond the scope of this study. Figure 4 shows the evolution of the signal over a typical cycle (Figure 4a) and the longer-term temporal evolution of the signal over the 101 year period of our analysis (Figures 4b–4d).

[16] We follow the spatial evolution of the signal at equally spaced snapshots (roughly 2.5 year intervals) through one half cycle. The initial snapshot (phase of 0) corresponds to peak negative domain-averaged PDSI conditions (i.e., domain-wide drought). The second half of the cycle is the mirror image of the first half cycle by construction, with the 180° phase pattern (roughly 10 year lag relative to initial phase of 0 snapshot), for example, reflecting the opposite conditions of those shown in the initial snapshot.

[17] The initial phase ( $\theta = 0^\circ$  and  $t = 0$  years) indicates strong domain-wide drought conditions, with particularly pronounced drought over the “Great Plains” region (i.e., the north central United States), the region most strongly associated with the Dust Bowl years of the 1930s. The most prominent feature in the associated SLP pattern is a large region of anomalously negative SLP over the subtropical and tropical sectors of the North Atlantic, indicative of a weakened summer Bermuda high. We interpret the Great Plains drought anomaly as arising from decreased moisture transport into the region because of the associated decrease in the land/ocean pressure gradient anomaly, which induces the decrease in southeasterly flow. Indeed, recent modeling results [*Schubert et al.*, 2004] suggest that an anomalously weak Bermuda high pressure confined to the summer and fall season has a key role in extreme drought events over the conterminous United States such as the Dust Bowl.

[18] As the signal evolves toward the “90°” phase pattern (roughly 5 year lag relative to the phase of 0 pattern), wet conditions are observed over the southwestern United States, resembling the characteristic pattern associated with El Niño discussed below. The corresponding SLP pattern of anomalous negative SLP anomalies in the subtropical eastern North Pacific suggests an ocean/land SLP gradient anomaly, implying increased moisture transport into the arid desert southwest and thus decreased drought conditions. Equivalently, this pattern indicates anomalous increase in drought in the southwestern United States

associated with a blocking high or “ridge” in the subtropical eastern North Pacific roughly 5 years before the phase of 0 pattern.

[19] This bidecadal signal projects onto notable peaks in mean drought for the conterminous United States (Figure 4b) in the 1930s (coinciding with the Dust Bowl) and, to a lesser extent, the 1950s and wet “pluvial” conditions during the 1940s. The severity of the 1930s drought is heightened by the lack of large interannual variations about the decadal trend, the latter being consistent with evidence discussed earlier from the evolutive MTM-SVD spectrum, of decreased interannual large-scale drought and atmospheric circulation variability at this time. Similar conclusions are evident in an examination of mean drought over the Great Basin region alone (Figure 4c). By contrast, and consistent with the spatial evolution of the signal discussed above, the signal projection onto southwestern U.S. drought (Figure 4d) indicates peak timing of drought/wet anomalies that precede those for the Great Basin by roughly 5 years (corresponding to roughly 90° of phase). It should be stressed that while the signal reconstruction only indicates slightly more than two coherent bidecadal cycles (and little variability early or late in the record), the significance (99% level, e.g., Figure 3c) of the signal derives from the existence of coherent evolving interrelated patterns of drought and atmospheric circulation at the bidecadal timescale and not simply the existence of roughly two coherent bidecadal cycles in, e.g., domain mean drought (i.e., Figure 4b) alone.

[20] Second, we examine the interannual timescale signal which is observed to be closely related to the influences of the El Niño–Southern Oscillation (ENSO). Past studies have indeed connected ENSO with significant hydroclimatic influences in North America during both the cold season [*Ropelewski and Halpert*, 1987; *Rajagopalan et al.*, 2000; *Piechota and Dracup*, 1996; *Trenberth and Branstator*, 1992; *Cole and Cook*, 1998; *Dai and Trenberth*, 1998] and the warm season [*Ting and Wang*, 1997; *Barlow et al.*, 2001]. Extreme hydrologic anomalies such as the 1988 drought and 1993 midwestern U.S. flooding events, for example, have been related to the influence of ENSO on the meridional displacement of the jet stream and mean storm track [*Bell and Janowiak*, 1995; *Trenberth and Guillemot*, 1996]. It is thus of interest to assess the relationship between the interannual signals detected in this study and other more conventional measures of the patterns of response of U.S. drought to ENSO.

[21] We focus specifically on the pattern associated with the roughly 5 year period variance peak shown in Figure 3. This is the most robust peak in the ENSO band detected in our analysis, significant at the 99% level in both the joint seasonal MTM-SVD analyses and the separate MTM-SVD

**Figure 4.** Reconstruction of bidecadal signal in U.S. summer drought/warm-season SLP. (a) Spatial reconstruction of signal showing patterns corresponding to phases  $\theta = 0^\circ$  (defined by maximum mean PDSI anomaly),  $45^\circ$  (one-eighth cycle is roughly 2.5 year lag),  $90^\circ$  (5 year lag),  $135^\circ$  (7.5 year lag), and  $180^\circ$  (10 year lag). Shown are normalized ( $z$  score) anomalies, color shaded for PDSI anomalies (warm colors indicate wet conditions, and cool colors indicate dry conditions) and contoured for SLP anomalies (cool colors indicate negative SLP anomalies, and warm colors indicate positive SLP anomalies). Also shown are the signal reconstruction (dashed lines) and raw data (solid lines) for (b) domain-averaged PDSI over the conterminous United States, (c) average PDSI for the Great Basin region ( $35^\circ$ – $50^\circ$ N,  $90^\circ$ – $110^\circ$ W), and (d) average PDSI for the southwestern United States ( $25^\circ$ – $35^\circ$ N,  $100^\circ$ – $125^\circ$ W).

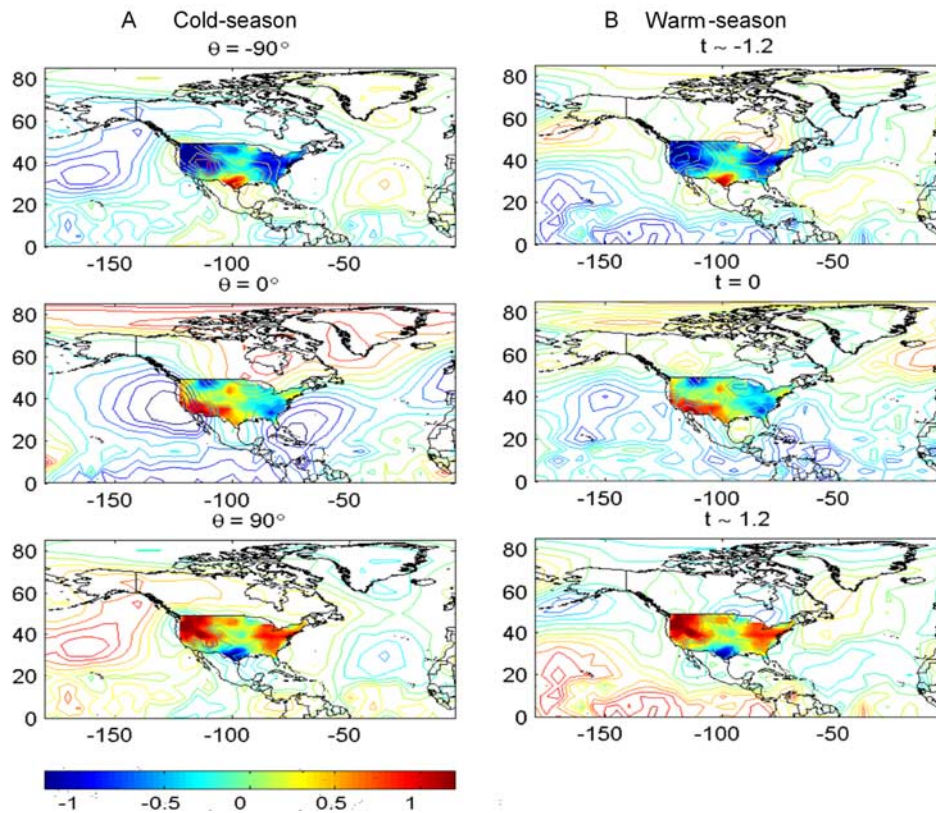


**Figure 5.** Spatial reconstructions of roughly 5 year timescale El Niño–Southern Oscillation (ENSO) signal showing patterns corresponding to phase  $\theta = 0^\circ$  (ENSO + 0, corresponding to timing of peak ENSO conditions),  $-90^\circ$  phase (ENSO – 1), and  $+90^\circ$  phase (ENSO + 1) for both (a) cold-season SLP/summer PDSI field and (b) warm-season SLP/summer PDSI field. Other conventions are as in Figure 4.

analysis (not shown) of the PDSI field only. We note, however, that the ENSO signal is certainly associated with a broader band of variance. In Figure 5 we show the typical spatial evolution of the roughly 5 year period signal over the 1895–1995 period of analysis, which demonstrates familiar established relationships between ENSO and extratropical atmospheric circulation changes in the Northern Hemisphere. The pattern of joint evolution of summer drought and SLP over a typical 5 year period event is shown in Figure 5 for both prior cold-season and current warm-season SLP. The “ENSO + 0” phase is defined to be coincident with the peak positive ENSO conditions (i.e., maximum negative projection of the signal onto the cold-season SOI) in both cases, while the conditions preceding that state by roughly 1 year (“ENSO – 1” defined by  $-90^\circ$  phase is  $-1.2$  year lag) and following that state by 1 year (“ENSO + 1” defined by  $+90^\circ$  phase is  $1.2$  year lag) are also shown. The evolving atmospheric circulation pattern is similar to that identified previously for joint patterns of evolution of Northern Hemisphere SLP and surface temperature at ENSO timescales [Mann and Park, 1996]. Consistent with other studies [e.g., Horel and Wallace, 1981], the low phase of the Southern Oscillation is observed to accompany notable cold-season circulation anomalies over the North Pacific and North America, with the initial stage (peak warm ENSO conditions) closely resembling the tropical–Northern Hemisphere extratropical teleconnection identified with ENSO in past work [Livezey and Mo, 1987].

The evolving structure of the North Pacific SLP anomalies can potentially be understood in terms of the slowly evolving tropical Pacific SST patterns associated with the ENSO cycle, which teleconnect to extratropical planetary waves through an “atmospheric bridge” [Lau and Nath, 1996; Trenberth et al., 1998; Alexander et al., 2002]. This signal reconstruction, which assumes a stationary description of the signal spatial evolution, could be generalized to examine nonstationary features in the signal evolution on the basis of a sequence of spatial reconstructions derived from independent 40 year intervals in the evolutive analysis described earlier. Such an extension of this analysis, however, is beyond the scope of this study.

[22] The evolving patterns of drought appear to be most closely tied to evolving cold-season synoptic-scale conditions, though the warm-season atmospheric circulation conditions also seem to play a role at certain phases of evolution of the signal. The “zero” phase of the signal indicates a familiar pattern of response of summer drought to warm ENSO events, with the southwestern United States and West Coast experiencing notable wet anomalies and with the northwestern and mid-Atlantic regions of the United States exhibiting moderate drought anomalies [Rajagopalan et al., 2000; Gershunov and Barnett, 1998; Cole and Cook, 1998]. The anomalous wetness is associated with an enhanced cold-season Aleutian Low and the associated anomalous advection of warm moist air into these regions because of an increased land/ocean SLP gradient

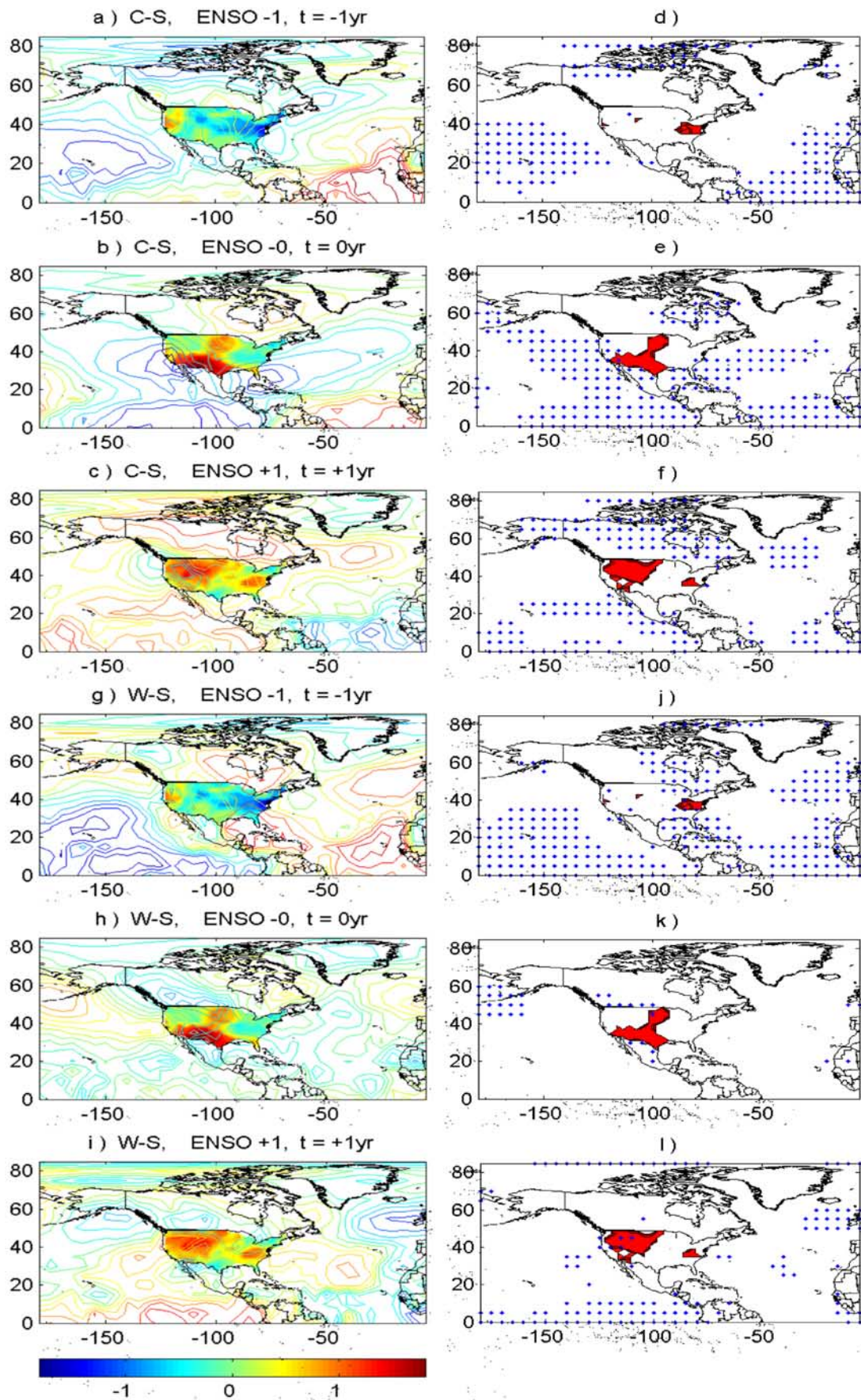


Figure 6

anomaly. Conversely, a weakened Bermuda high pressure is consistent with anomalous advection of cold, dry continental air into the southeastern and mid-Atlantic regions of the United States. The serial persistence implicit in the definition of summer drought [Palmer, 1965] combined with potential positive soil moisture feedbacks [Namias, 1989; Wolfson *et al.*, 1987; Mo *et al.*, 1997; Hong and Kalnay, 2000] leads to persistence in the associated drought/wet response. In particular, enhanced/diminished cold-season precipitation associated with warm events leads to enhanced/diminished soil moisture/snowfall that translates to diminished/enhanced warm-season drought conditions.

[23] The region of anomalously wet conditions along the West Coast of the United States follows the migration of the anomalous negative SLP anomaly in the North Pacific as the signal evolves during the first year following the warm event (ENSO + 1 phase). An anomalous wet signal develops over the eastern United States in apparent response to the development of an anomalous southeastward displaced Bermuda high, which appears in both the prior cold and concurrent warm seasons. Drought conditions that develop over the south central United States within roughly 1 year relative to peak ENSO conditions also appear to reflect this migration of the Bermuda high, with the warm-season atmospheric circulation suggesting decreased inflow of moist Gulf of Mexico air, assisted by an anomalous ridge in the subtropical North Pacific. The relationship between ENSO and central United States drought is similar to that identified in previous studies [e.g., Ting and Wang, 1997; Barlow *et al.*, 2001].

[24] The use of a frequency domain approach to characterizing ENSO influences is limited in certain respects. Cold-event (La Niña) influences are implicitly defined as the reverse of warm-event (El Niño) influences. Furthermore, if only one mode (e.g., as in our case, the 5 year period mode) is retained, then the implicit characterization is one of a stationary pattern of evolution from one event to another. However, there is some evidence that the pattern of hydroclimatic response to ENSO over the conterminous United States may be modulated by other climate processes such as the “Pacific Decadal Oscillation” or “PDO” on longer timescales [e.g., Cole and Cook, 1998; Gershunov and Barnett, 1998]. We thus test the robustness of our earlier conclusions through the use of a more elementary compositing approach [see, e.g., Ropelewski and Halpert, 1987] to describe the typical patterns of drought and SLP in the year preceding (ENSO - 1), coinciding with (ENSO - 0), and following (ENSO + 1) El Niño and La Niña events. We defined the ENSO events by years within the 1900–1995 interval for which the absolute value of the cold-season SOI exceeds the long-term mean by  $\pm 1\sigma$  standard deviation. This yields the following list of (13) El Niño events: 1904, 1905, 1911, 1914, 1918, 1925, 1940, 1965, 1977, 1982, 1986, 1991, and 1992. It also yields the following list of (14) La Niña events: 1903, 1909, 1916,

1917, 1924, 1928, 1938, 1949, 1950, 1955, 1970, 1973, 1975, and 1988.

[25] We computed composites of the PDSI and SLP fields after removal of the estimated projections of other modes of variability arguably independent of ENSO through linear regression against the cold-season (November–April) North Atlantic Oscillation [e.g., Jones *et al.*, 1997] and cold-season PDO [Mantua *et al.*, 1997] indices. Computations without employing this latter step (not shown) yielded very similar results, suggesting that ENSO indeed is the dominant determinant of changing U.S. drought patterns on interannual timescales.

[26] The composite ENSO signal was then defined by the difference between the composites of the warm-event (El Niño) and cold-event (La Niña) years (note that any years for which the cold-season SOI exceeds the long-term mean by  $\pm 1\sigma$  standard deviation were eliminated from consideration as ENSO - 1 or ENSO + 1 years). A Monte Carlo procedure was used in determining the significance of composite ENSO signals, based on the use of randomly selected event lists of the same length as the event lists employed in the actual composites. Five thousand Monte Carlo surrogates were used to obtain a two-tailed null distribution for the ENSO - 0, ENSO - 1, and ENSO + 1 anomaly values, and appropriate significance levels were diagnosed from this null distribution.

[27] The results of this analysis (Figure 6) display a striking similarity to those obtained with the MTM-SVD analysis (Figure 5). The cold-season peak ENSO signal (ENSO - 0) shows the same basic features as the corresponding MTM-SVD (phase of 0 in Figure 5) pattern, though the composite pattern shows a stronger and somewhat more coherent pattern of drought through the southern and central United States that is highly significant (exceeding 99% level). A close correspondence exists between the ENSO + 1 composite and the 90° phase pattern (corresponding roughly to +1 year relative to peak warm-event conditions) with significant wetness, for example, over the northwest United States. Differences are found over the North Atlantic Ocean (for which the ENSO response is least robust and more likely influenced by noise and the details of the signal estimation methodology). As in the MTM-SVD results, the warm-season SLP signals appear less closely tied to summer drought anomalies, with possible exceptions in the eastern and south central United States.

## 5. Conclusions

[28] A joint analysis of Northern Hemisphere seasonal SLP and conterminous U.S. summer drought based on the MTM-SVD method yields evidence of coherent oscillatory patterns of variability in continental U.S. drought on interannual and bidecadal timescales. In many cases the timescales are consistent with those identified in previous

**Figure 6.** Observational spatial patterns of ENSO-related anomalies for ENSO - 1, ENSO - 0, and ENSO + 1 for both (a–c) cold-season SLP/summer PDSI field as well as (d–f) their confidence levels and (g–i) warm-season SLP/summer PDSI field as well as (j–l) their confidence levels. For composite patterns, conventions are as in Figures 4 and 5. For confidence levels, blue dots indicate statistically significant ( $p < 0.1$  for a two-tailed test) SLP anomalies while red area indicates significant PDSI anomalies.

analyses of various Northern Hemisphere climate fields. A bidecadal drought signal previously detected in reconstructed North American summer drought patterns of the past few centuries is isolated in our analysis of twentieth century summer drought and coupled warm-season atmospheric circulation/drought relationships. This signal is associated with the 1930s Dust Bowl and a similar, though lesser, large-scale drought anomaly during the 1950s. On interannual timescales we identify coupled modes of summer drought and seasonal SLP consistent with ENSO influences. The spatial patterns of the associated signal show a close relationship between evolving cold-season synoptic-scale atmospheric circulation changes associated with various phases of ENSO and hydroclimatic conditions that ultimately have a large influence on summer continental drought patterns. A weaker relationship is evident between summer drought and concurrent summer season atmospheric circulation conditions. An alternative compositing approach yields a similar picture of the relationship between atmospheric circulation changes associated with various stages of the ENSO cycle and summer drought patterns. In this study, we have focused on the identification of dynamically consistent patterns of atmospheric circulation and drought variability. A useful future extension of this study might seek to establish possible forcing of such patterns by, e.g., both tropical Pacific [e.g., Hoerling and Kumar, 2003] and Atlantic [Schubert et al., 2004; McCabe et al., 2004] SST forcing. Such an extension would be accommodated through the inclusion of SST data in the joint analysis. The continued investigation of potential climate signals impacting variations in continental drought on interannual and decadal timescales could lead to improved long-lead hydroclimatic forecasting over the conterminous United States.

[29] **Acknowledgment.** This work was supported by the NSF- and NOAA-funded "Earth Systems History" program (NOAA grant NA96GP0404).

## References

- Alexander, M. A., I. Bladé, M. Newman, J. R. Lanzante, N.-C. Lau, and J. D. Scott (2002), The atmospheric bridge: The influence of ENSO teleconnections on air-sea interaction over the global oceans, *J. Clim.*, *15*, 2205–2231.
- Allen, M. R., and L. A. Smith (1994), Investigating the origins and significance of low-frequency modes of climate variability, *Geophys. Res. Lett.*, *21*, 883–886.
- Barlow, M., S. Nigam, and E. H. Berbery (2001), ENSO, Pacific decadal variability, and U.S. summertime precipitation, drought, and stream flow, *J. Clim.*, *14*, 2105–2128.
- Barnett, T. P. (1991), The interaction of multiple time scales in the tropical climate system, *J. Clim.*, *4*, 269–285.
- Basnett, T. A., and D. E. Parker (1997), Development of the global mean sea level pressure data set GMSLP2, *Clim. Res. Tech. Note CRTN 79*, Hadley Cent., Exeter, U.K.
- Bell, G. D., and J. E. Janowiak (1995), Atmospheric circulation associated with the Midwest floods of 1993, *Bull. Am. Meteorol. Soc.*, *76*, 681–695.
- Cole, J., and E. Cook (1998), The changing relationship between ENSO variability and moisture balance in the continental United States, *Geophys. Res. Lett.*, *25*, 4529–4532.
- Cook, E. R., D. M. Meko, and C. W. Stockton (1997), A new assessment of possible solar and lunar forcing of the bidecadal drought rhythm in the western United States, *J. Clim.*, *10*, 1343–1456.
- Cook, E. R., D. M. Meko, D. W. Stahle, and M. K. Cleaveland (1999), Drought reconstructions for the continental United States, *J. Clim.*, *12*, 1145–1162.
- Dai, A., and K. E. Trenberth (1998), Global variation in droughts and wet spells, *Geophys. Res. Lett.*, *25*, 3367–3370.
- Delworth, T. L., and M. E. Mann (2000), Observed and simulated multi-decadal variability in the Northern Hemisphere, *Clim. Dyn.*, *16*, 661–676.
- Dettinger, M. D., M. Ghil, and C. L. Keppenne (1995), Interannual and interdecadal variability in United States surface-air temperatures, *Clim. Change*, *31*, 35–66.
- Gershunov, A., and T. P. Barnett (1998), Interdecadal modulation of ENSO teleconnections, *Bull. Am. Meteorol. Soc.*, *79*, 2715–2725.
- Ghil, M., and R. Vautard (1991), Interdecadal oscillations and the warming trend in global temperature time series, *Nature*, *350*, 324–327.
- Hoerling, M., and A. Kumar (2003), The perfect ocean for drought, *Science*, *299*, 691–694.
- Hong, S.-Y., and E. Kalnay (2000), Role of sea surface temperature and soil-moisture feedback in the 1998 Oklahoma-Texas drought, *Nature*, *408*, 842–844.
- Horel, J. D. (1981), A rotated principal component analysis of the inter-annual variability of the Northern Hemisphere 500 mb height field, *Mon. Weather Rev.*, *109*, 2080–2092.
- Horel, J. D., and J. M. Wallace (1981), Planetary-scale atmospheric phenomena associated with Southern Oscillation, *Mon. Weather Rev.*, *109*, 813–829.
- Jiang, N., J. D. Neelin, and M. Ghil (1995), Quasi-quadrennial and quasi-biennial variability in the equatorial Pacific, *Clim. Dyn.*, *12*, 101–112.
- Jones, P. D., T. Jonsson, and D. Wheeler (1997), Extension to the North Atlantic Oscillation using early instrumental pressure observations from Gibraltar and south-west Iceland, *Int. J. Climatol.*, *17*, 1433–1450.
- Kalnay, E., et al. (1996), The NCEP/NCAR 40-year Reanalysis Project, *Bull. Am. Meteorol. Soc.*, *77*, 437–471.
- Kaplan, A., Y. Kushnir, M. A. Cane, and M. B. Blumenthal (1997), Reduced space optimal analysis for historical data sets: 136 years of Atlantic sea surface temperatures, *J. Geophys. Res.*, *102*, 27,835–27,860.
- Kaplan, A., M. A. Cane, Y. Kushnir, and A. C. Clement (1998), Analyses of global sea surface temperature 1856–1991, *J. Geophys. Res.*, *103*, 18,567–18,589.
- Kaplan, A., Y. Kushnir, and M. A. Cane (2000), Reduced space optimal interpolation of historical marine sea level pressure, *J. Clim.*, *13*, 2987–3002.
- Keppenne, C. L., and M. Ghil (1992), Adaptive filtering and prediction of the Southern Oscillation Index, *J. Geophys. Res.*, *97*, 20,449–20,454.
- Lall, U., and M. E. Mann (1995), The Great Salt Lake: A barometer of low-frequency climatic variability, *Water Resour. Res.*, *31*, 2503–2515.
- Lau, N.-C., and M. J. Nath (1996), The role of the "atmospheric bridge" in linking tropical Pacific ENSO events to extratropical SST anomalies, *J. Clim.*, *9*, 2036–2057.
- Livezey, R. E., and K. C. Mo (1987), Tropical-extratropical teleconnections during the Northern Hemisphere winter. Part II: Relationships between monthly mean Northern Hemisphere circulation patterns and proxies for tropical convection, *Mon. Weather Rev.*, *115*, 3115–3132.
- Mann, M. E., and J. Park (1993), Spatial correlations of interdecadal variation in global surface temperatures, *Geophys. Res. Lett.*, *20*, 1055–1058.
- Mann, M. E., and J. Park (1994), Global scale modes of surface temperature variability on interannual to century time scales, *J. Geophys. Res.*, *99*, 25,819–25,833.
- Mann, M. E., and J. Park (1996), Joint spatio-temporal modes of surface temperature and sea level pressure variability in the Northern Hemisphere during the last century, *J. Clim.*, *9*, 2137–2162.
- Mann, M. E., and J. Park (1999), Oscillatory spatiotemporal signal detection in climate studies: A multiple-taper spectral domain approach, *Adv. Geophys.*, *41*, 1–131.
- Mann, M. E., and S. Rutherford (2002), Climate reconstruction using "Pseudoproxies," *Geophys. Res. Lett.*, *29*(10), 1501, doi:10.1029/2001GL014554.
- Mann, M. E., U. Lall, and B. Saltzman (1995a), Decadal-to-century scale climate variability: Insights into the rise and fall of the Great Salt Lake, *Geophys. Res. Lett.*, *22*, 937–940.
- Mann, M. E., J. Park, and R. S. Bradley (1995b), Global interdecadal and century-scale climate oscillations during the past five centuries, *Nature*, *378*, 266–270.
- Mann, M. E., R. S. Bradley, and M. K. Hogue (2000), Long-term variability in the El Niño Southern Oscillation and associated teleconnections, in *El Niño and the Southern Oscillation: Multiscale Variability and its Impacts on Natural Ecosystems and Society*, edited by H. F. Diaz and V. Markgraf, pp. 357–412, Cambridge Univ. Press, New York.
- Mantua, N. J., S. R. Hare, Y. Zhang, J. M. Wallace, and R. C. Francis (1997), A Pacific interdecadal climate oscillation with impacts on salmon production, *Bull. Am. Meteorol. Soc.*, *78*, 1069–1079.
- McCabe, G., M. Palecki, and J. L. Betancourt (2004), Pacific and Atlantic Ocean influences on multi-decadal drought frequency in the United States, *Proc. Natl. Acad. Sci. U. S. A.*, *101*, 4136–4141.
- Minobe, S. (2000), Spatio-temporal structure of the pentadecadal variability over the North Pacific, *Prog. Oceanogr.*, *47*, 381–408.

- Mo, K. C., J. N. Paegle, and R. W. Higgins (1997), Atmospheric processes associated with summer floods and droughts in the central United States, *J. Clim.*, *10*, 3028–3046.
- Moron, V., R. Vautard, and M. Ghil (1998), Trends, interdecadal and interannual oscillations in global sea-surface temperature, *Clim. Dyn.*, *14*, 545–569.
- Namias, J. (1989), Cold waters and hot summer, *Nature*, *338*, 15–16.
- Newman, M., G. P. Compo, and M. A. Alexander (2004), ENSO-forced variability of the Pacific Decadal Oscillation, *J. Clim.*, *16*, 3853–3857.
- Nicholls, N. (1988), El Niño-Southern Oscillation impact prediction, *Bull. Am. Meteorol. Soc.*, *69*, 173–176.
- Palmer, W. C. (1965), Meteorological drought, *Weather Bur. Res. Pap.* *45*, 58 pp., U.S. Dep. of Commer., Washington, D. C.
- Park, J., and M. E. Mann (2000), Interannual temperature events and shifts in global temperature: A “multiwavelet” correlation approach, *Earth Interact.*, *4*, pap. 1, 36 pp.
- Piechota, T. C., and J. A. Dracup (1996), Drought and regional hydrologic variation in the United States: Associations with the El Niño–Southern Oscillation, *Water Resour. Res.*, *32*, 1359–1370.
- Rajagopalan, B., Y. Kushnir, and Y. M. Tourre (1998a), Observed decadal midlatitude and tropical Atlantic climate variability, *Geophys. Res. Lett.*, *25*, 3967–3970.
- Rajagopalan, B., M. E. Mann, and U. Lall (1998b), A multivariate frequency-domain approach to long-lead climatic forecasting, *Weather Forecast.*, *13*, 58–74.
- Rajagopalan, B., E. R. Cook, U. Lall, and K. R. Bonnie (2000), Spatio-temporal variability of ENSO and SST teleconnections to summer drought over the United States during the twentieth century, *J. Clim.*, *13*, 4244–4255.
- Ribera, P., and M. E. Mann (2002), Interannual variability in the NCEP Reanalysis 1948–1999, *Geophys. Res. Lett.*, *29*(10), 1494, doi:10.1029/2001GL013905.
- Ribera, P., and M. E. Mann (2003), ENSO related variability in the Southern Hemisphere, 1948–2000, *Geophys. Res. Lett.*, *30*(1), 1006, doi:10.1029/2002GL015818.
- Ropelewski, C. F., and M. S. Halpert (1987), Global and regional scale precipitation patterns associated with the El Niño/Southern Oscillation, *Mon. Weather Rev.*, *115*, 1606–1626.
- Rutherford, S., M. E. Mann, T. L. Delworth, and R. Stouffer (2003), Climate field reconstruction under stationary and nonstationary forcing, *J. Clim.*, *16*, 462–479.
- Schneider, T. (2001), Analysis of incomplete climate data: Estimation of mean values and covariance matrices and imputation of missing values, *J. Clim.*, *14*, 853–871.
- Schubert, S. D., M. J. Suarez, P. J. Pegion, R. D. Koster, and J. T. Bacmeister (2004), On the cause of the 1930s Dust Bowl, *Science*, *303*, 1855–1859.
- Smith, T. M., R. W. Reynolds, R. E. Livezey, and D. C. Stokes (1996), Reconstruction of historical sea surface temperatures using empirical orthogonal functions, *J. Clim.*, *9*, 1403–1420.
- Ting, M., and H. Wang (1997), Summertime U.S. precipitation variability and its relation to Pacific sea surface temperature, *J. Clim.*, *10*, 1853–1873.
- Tourre, Y. M., and W. B. White (2003), Patterns of coherent climate signals in the Indian Ocean during the 20th century, *Geophys. Res. Lett.*, *30*(23), 2224, doi:10.1029/2003GL018476.
- Tourre, Y. M., B. Rajagopalan, Y. Kushnir, M. Barlow, and W. B. White (2001), Patterns of coherent decadal and interdecadal climate signals in the Pacific Basin during the 20th century, *Geophys. Res. Lett.*, *28*, 2069–2072.
- Trenberth, K. E., and G. W. Branstator (1992), Issues in establishing causes of the 1988 drought over North America, *J. Clim.*, *5*, 159–172.
- Trenberth, K. E., and C. J. Guillemot (1996), Physical processes involved in the 1988 drought and 1993 floods in the North America, *J. Clim.*, *9*, 1288–1298.
- Trenberth, K. E., and J. W. Hurrell (1994), Decadal atmosphere-ocean variations in the Pacific, *Clim. Dyn.*, *9*, 303–319.
- Trenberth, K. E., and D. A. Paolino Jr. (1980), The Northern Hemisphere sea-level pressure data set: Trends, errors and discontinuities, *Mon. Weather Rev.*, *108*, 855–872.
- Trenberth, K. E., G. W. Branstator, D. Karoly, A. Kumar, N.-C. Lau, and C. Ropelewski (1998), Progress during TOGA in understanding and modeling global teleconnections associated with tropical sea surface temperatures, *J. Geophys. Res.*, *103*, 14,291–14,324.
- Venegas, S. A., M. R. Drinkwater, and G. Shaffer (2001), Coupled oscillations in Antarctic sea ice and atmosphere in the South Pacific sector, *Geophys. Res. Lett.*, *28*, 3301–3304.
- Wallace, J. M., and D. S. Gutzler (1981), Teleconnection in the geopotential height field during the Northern Hemisphere winter, *Mon. Weather Rev.*, *109*, 784–812.
- White, W. B., and D. R. Cayan (1998), Quasi-periodicity and global symmetries in interdecadal upper ocean temperature variability, *J. Geophys. Res.*, *103*, 21,335–21,354.
- Wolfson, N., R. Atlas, and Y. C. Sud (1987), Numerical experiments related to the summer 1980 heat wave, *Mon. Weather Rev.*, *115*, 1345–1357.
- Zhang, Z., M. E. Mann, and E. R. Cook (2004), Alternative methods of proxy-based climate field reconstruction: Application to summer drought over the conterminous United States back to AD 1700 from tree-ring data, *Holocene*, *14*, 502–516.
- Zorita, E., F. González-Rouco, and S. Legutke (2003), Testing the Mann et al. (1998) approach to paleoclimate reconstructions in the context of a 1000-yr control simulation with the ECHO-G coupled climate model, *J. Clim.*, *16*, 1378–1390.

---

M. E. Mann and Z. Zhang, Department of Environmental Sciences, University of Virginia, Charlottesville, VA 22904-4123, USA. (zz9t@virginia.edu)